Cellular and Molecular Life Sciences (2023) 80:363
https://doi.org/10.1007/s00018-023-05006-0

ORIGINAL ARTICLE

Polymorphic USP8 allele promotes Parkinson's disease by inducing the accumulation of α-synuclein through deubiquitination

Shouhai Wu[1,2] · Tongxiang Lin[2,3] · Yang Xu[4]

Received: 7 July 2023 / Revised: 14 October 2023 / Accepted: 16 October 2023 / Published online: 19 November 2023

Abstract

Parkinson's disease (PD) is one of the most common neuro-degenerative diseases characterized by α-synuclein accumulation and degeneration of dopaminergic neurons. Employing genome-wide sequencing, we identified a polymorphic USP8 allele ($USP8^{D442G}$) significantly enriched in Chinese PD patients. To test the involvement of this polymorphism in PD pathogenesis, we derived dopaminergic neurons (DAn) from human-induced pluripotent stem cells (hiPSCs) reprogrammed from fibroblasts of PD patients harboring $USP8^{D442G}$ allele and their healthy siblings. In addition, we knock-in D442G polymorphic site into the endogenous USP8 gene of human embryonic stem cells (hESCs) and derived DAn from these knock-in hESCs to explore their cellular phenotypes and molecular mechanism. We found that expression of $USP8^{D442G}$ in DAn induces the accumulation and abnormal subcellular localization of α-Synuclein (α-Syn). Mechanistically, we demonstrate that D442G polymorphism enhances the interaction between α-Syn and USP8 and thus increases the K63-specific deubiquitination and stability of α-Syn . We discover a pathogenic polymorphism for PD that represent a promising therapeutic and diagnostic target for PD.

Keywords Rs3743044 · CRISPR/Cas9 · Protein structure · Disease prediction

Abbreviations

α-Syn	Alpha synuclein
USP8	Ubiquitin specific protease-8
WT	Wild type
MT	USP8 D442G mutation
PD	Parkinson's disease
IP	Immunoprecipitation
IB	Immunoblotting
WB	Western blot
DUBs	Deubiquitinases
IF	Immunofluorescence
TH	Tyrosine hydroxylase
TUJ1	Tubulin beta 3 class III
iPSC	Induced pluripotent stem cells
NSC	Neural stem cells
hESC	Human embryonic stem cell
DAn	Midbrain dopaminergic neuron cell
EV	Empty vector

✉ Yang Xu
xuyang2020@zju.edu.cn

1 State Key Laboratory of Dampness Syndrome of Chinese Medicine, The Second Affiliated Hospital of Guangzhou University of Chinese Medicine, Guangzhou, China

2 Center for Regenerative and Translational Medicine, Guangdong Provincial Academy of Chinese Medical Sciences, The Second Affiliated Hospital of Guangzhou University of Chinese Medicine, Guangzhou, China

3 College of Animal Sciences, Fujian Agriculture and Forestory University, 15 ShangXiaDian Road, CangShan District, Fuzhou City, Fujian Province, China

4 Department of Cardiology, Cardiovascular Key Lab of Zhejiang Province, State Key Laboratory of Transvascular Implantation Devices, The Second Affiliated Hospital, Zhejiang University School of Medicine, Zhejiang University, Hangzhou 310009, Zhejiang, China

Introduction

Parkinson's disease (PD) is one of the most devastating neurodegenerative diseases without any effective treatment. While the mechanisms of pathogenesis remain unclear, extensive studies have shown that many genetic and environmental factors are involved in the PD development [1]. One of the key challenges in studying PD is the lack of access to the brain tissue samples from PD patients and healthy controls. Induced pluripotent stem cells (iPSC) derived from PD patients offer a unique opportunity to study the pathogenesis of PD [2]. In

this context, DAn derived from the PD hiPSCs offer a unique "disease in a dish" model to study the pathogenesis of PD and screen therapeutic strategies to reverse the pathogenesis.

Ubiquitination–deubiquitination is an important mechanism of proteolysis to regulate protein stability [3]. Most cellular proteins are selectively targeted for degradation by conjugating to a ubiquitin chain [4]. The formation of ubiquitin chain at K48 or K11 residues causes the 26S proteasome to degrade the cytosolic proteins, while the ubiquitin chain linked to the membrane-bound proteins at K63 target the proteins for lysosomal degradation [5]. Previous findings implicate important roles of ubiquitin-specific proteases in neurodegeneration [6]. For example, USP14 and ovarian tumor ubiquitin Aldehyde binding (OTUB)-1 can regulate the deubiquitination of tau and its clearance by the proteasome [7, 8]. USP13 can regulate α-Syn ubiquitination in α-synucleinopathies [9]. USP8 can remove the K63-linked ubiquitin chains on α-Syn and reduces its lysosomal degradation in DAn [10]. The impaired clearance and accumulation of these neurotoxic proteins, including α-Syn, can play key roles in inducing neurodegeneration [11].

In this study, we discovered a pathogenic polymorphism ($USP8^{D442G}$) of USP8 allele associated with Chinese PD patients. The expression of $USP8^{D442G}$ in DAn drives the pathogenic accumulation of α-Syn, which can be reversed by the ectopic expression of $USP8^{D442}$. Mechanistically, we discovered that D442G polymorphism increases the interaction between USP8 and α-Syn to inhibit the degradation and promote the accumulation of α-Syn in DAn neurons, suggesting that this polymorphism is pathogenic. Therefore, $USP8^{D442G}$ allele could serve as a new diagnostic biomarker for PD and present a new therapeutic target to treat PD.

Materials and methods

Reprogram of human skin fibroblasts into integration-free iPSCs

Skin biopsy pieces (2 mm diameter) were taken from patients or healthy siblings with informed consent under the guidance and approval of the Guangdong Provincial Hospital of Traditional Chinese Medicine (TCM) Board of Ethics. Biopsy samples were kept in 10×penicillin/streptomycin (pen/strep; Invitrogen, USA) for 10 min and then washed with phosphate-buffered saline (PBS). Biopsy samples were cut into four pieces and cultured with MEF medium (Dulbecco's modified Eagles medium (DMEM), 10% fetal bovine serum (FBS), 1×pen/strep) in a T25 flask. The culture medium was changed every 3 days. When cultures were 80–90% confluent, cells were trypsinized and passaged. Then derived iPSCs, we used a Nucleotransfection Kit (P2 primary cell 4D-Nucleotector X Kit, Lonza) to transfect the Y4 episomal vectors (pCXLE-hOCT3/4-shp53, pCXLE-hSK and pCXLE-hUL, Okita et al. Nat Methods. 2011) [12] to the fibroblasts with the procedure of DT-130. Cells were transfected with 2 μg of the aforementioned vectors per transfection in a volume of 100 μL. The ratio of Nucleofector Solution: DNA was 4.5:1. Then, the human fibroblast cells were cultured for 2 days. Cultures were trypsinized and seeded into 6-well plates coated with Matrigel (30,000 cells/well). Cells were cultured in ESC medium containing DMEM/F12 (Gibco, 11330), KnockOut™ Serum Replacement (Gibco), MEM non-essential amino acids (Gibco), L-glutamine (Gibco), 55 mM β-mercaptoethanol (Gibco) and 20ng bFGF (Gibco), on feeders which were taken from CF1 mouse embryos and subjected to irradiation with the dose of 30 Gy. Clones with hESC morphology appeared between day 25 and 45. They were picked and expanded under hESC culture condition. We generated 2–8 independent iPSC lines per fibroblast samples, PD1-PD5, and the siblings' healthy control of PD3 and PD4 (PD3C and PD4C).

Directed differentiation of iPSCs to midbrain DA neurons

The iPSCs were differentiated to midbrain DA neurons based on a directed differentiation protocol [13, 14] with two improvements. iPS cells at a higher density of 1.5×10^6 per well were seeded when initializing the neuronal differentiation. After 11 days, cultures were passaged into plates coated sequentially with 1:10 Poly-L-ornithine solution in double distilled H_2O (Sigma-Aldrich, P4957) and 0.3 mg/mL Matrigel Matrix (BD Biosciences, 3542777). The medium contains DMEM-F12: Neurobasal (1:1), 1×N2 (Gibco), 1×B27 (Gibco), 1% glutmax (Gibco), 5 ng/mL BSA, 10 ng/mL hLIF (Millipore), and to become neural stem cell (NSC) with LDN193189 (100 nM, Sigma-Aldrich), SB431542 (2 μM, Tocris), CHIR99021 (3 μM, Sigma-Aldrich). We performed the FACS using a combination of antibodies to NSC surface markers, CD133 (CD133-APC, BD Pharmingen-566596) and CD56 (CD56-PE, BD Pharmingen-563238). Differentiated cell cultures were dissociated with Accutase (Gibco), neutralized with an equal volume of media and transferred into 15 mL conical tube. After spinning at 800 RPM for 5 min, the cell pellet was re-suspended in FACS buffer (DPBS + 0.5% BSA Fraction V, 2mM EDTA, 20 mM Glucose, and 100 U/mL Penicillin–Streptomycin), and filtered through a BD Falcon polypropylene 12×75 mm Clear Tube with cell strainer cap. Cell suspensions were then incubated in antibody cocktail (CD133-APC and CD56-PE), diluted 1:100 in FACS buffer for 15 min at 25 ℃ protected from light. Excess antibodies were washed off and cells were re-suspended in 1–3 mL FACS buffer prior to flow cytometry. We performed the Sorting used the Flow Cytometry (BD FACSAria III) with the 85 μm Nozzle-Configuration and Purity Mode. The

post-sorted NSCs were maintained in original medium and cultured. After 3–5 days, the NSCs were passaged and the medium was changed to NB medium containing Neurobasal medium with 100 ng/mL SHH (C24II, Miltenyi Biotec), 100 ng/mL FGF8b (Peprotech), 10ng/mL BDNF (Peprotech), 10 ng/mL GDNF (Peprotech), 0.2 mM ascorbic acid (Sigma-Aldrich), 1 ng/mL TGF-β3 (Peprotech), 0.5 mM dibutyryl-cAMP (Sigma-Aldrich), 10 mM DAPT (Sigma-Aldrich), 1 × N2 and 1 × B27 for 10 days. On days about 25, cells were dissociated using Accutase and sorted with CD15 (CD15-APC, BD Pharmingen-551376)/CD184 (CD184-PE-Cy5, BD Pharmingen-555975) double negative and CD24 (CD24-PE, BD Pharmingen-560991)/CD56 (CD56-PE-Cy7, BD Pharmingen-557747) double positive cell population by FACS with the method similar to sorting the NSCs. In order to better protect the synapses of nerve cells, we used the 100 μm Nozzle-Configuration and Purity Mode when cell sorting. The sorted cells were then cultured in final differentiation medium for 10 days until day 35 before any given experiment.

Characterization of hiPSCs

The iPS cells were stained with SSEA4 (Stemgent), OCT4 (BD Pharmingen) and TRA-1-81 (Millipore) through IF, cell nuclei were counterstained with DAPI. Alkaline phosphatase activity was detected using an Leukocyte Alkaline Phosphatase Kit (Sigma 86R ALP). The marker genes expression was detected by RT-PCR with primer pairs specific to human Oct4, Nanog and Sox2. Results were normalized using the comparative C (T) method and compared with equivalent values determined from H9-ESC (positive control) and non-transduced human fibroblasts (negative control), the primers are shown in Table 1. Exogenous DNA integration was detected by the same method, and RT-PCR reactions were carried out and normalized to GAPDH. the primers are described in Table 1. Teratoma assays were carried out to detect the ability of iPSCs to differentiate into triploderm. We injected $3–5 \times 10^6$ cells along with Matrigel under the kidney capsule of NOD/SCID mice. After 6–8 weeks, tumors were excised, fixed with 4% (v/v) paraformaldehyde, and their histology analyzed. The animal use was approved by the Board of Animal Research Committee of Guangdong Hospital of TCM.

Characterization of hiPSC-derived NSCs and DAn

RT-PCR was used to detected the NSC marker gene, NESTIN and PAX6, mRNA expression in the NSC pre-soring and NSC-post-sorting, and the iPSC marker-gene, Naong, Oct4 and Sox2 to examine the cells' differentiation compared with the control iPSCs. The primers are described in Table 1. Simultaneously, the post-NSC cells were stained with NESTIN (Anti-NESTIN antibody, abcam-ab105389) and PAX6 (Anti-PAX6 antibody, abcam-ab78545) by IF. The characterization of DAn by cell morphology, DAn-marker gene

Table 1 Primers for qPCR

Gene	Forward (5′ to 3′)	Reverse (5′ to 3′)
GAPDH	CGGAGTCAACGGATTTGGTC	GACAAGCTTCCCGTTCTCAG
$USP8^{total}$	GTCCAGGAGTCACTGCTAGTT	AGGAGCCAGTTTTCATAGCCT
$USP8^{D442}$	CAGTTGAACCAGTTGCTGCT	CTGGCTTGGTGGAACGAT
$USP8^{D442G}$	CAGTTGAACCAGTTGCTGCT	CTGGCTTGGTGGAACGAC
hOct4	GACAGGGGGAGGGGAGGAGCTAGG	CTTCCCTCCAACCAGTTGCCCCAAAC
hSox2	GGGAAATGGGAGGGGTGCAAAAGAGG	TTGCGTGAGTGTGGATGGGATTGGTG
hNanog	CAGCCCCGATTCTTCCACCAGTCCC	CGGAAGATTCCCAGTCGGGTTCACC
OCT3/4(CDS)	CCCCAGGGCCCCATTTTGGTACC	ACCTCAGTTTGAATGCATGGGAGAGC
OCT3/4(pla)	CATTCAAACTGAGGTAAGGG	TAGCGTAAAAGGAGCAACATAG
SOX2(CDS)	TTCACATGTCCCAGCACTACCAGA	TCACATGTGTGAGAGGGGCAGTGTGC
SOX2(pla)	TTCACATGTCCCAGCACTACCAGA	TTTGTTTGACAGGAGCGACAAT
EBNA	ATCAGGGCCAAGACATAGAGATG	GCCAATGCAACTTGGACGTT
PAX6	TGGGCAGGTATTACGAGACTG	ACTCCCGCTTATACTGGGCTA
NESTIN	CTGCTACCCTTGAGACACCTG	GGGCTCTGATCTCTGCATCTAC
TUJ1	GCCTCTTCTCACAAGTACGTGCCTCG	GGGGCGAAGCCGGGCATGAACAAGTGCAG
TH	GCCCTACCAAGACCAGACGTA	CGTGAGGCATAGCTCCTGAG
FOXA2	GGGAGCGGTGAAGATGGA	TCATGTTGCTCACGGAGGAGTA
PITX3	GTGCGGGTGTGGTTCAAGAA	AGCTGCCTTTGCATAGCTCG
NEUN	CCCATCCCGACTTACGGAG	GCTGAGCGTATCTGTAGGCT

mRNA and protein expression and cell electrophysiological detection. RT-PCR quantitative gene-expression in DAn pre-sorting and DAn post-sorting was compared with NSC post-sorting. IF for DAn markers TH, TUJ1, FOXA2 and MAP2 was performed to confirm the midbrain dopaminergic lineage on days 5 post-sorting.

Recordings of synaptic and ionic currents were performed with standard whole-cell voltage-clamp techniques. For whole-cell patch clamp experiments, neurons derived from iPSCs were plated on 35 mm petri-dishes. Recordings of cultured neurons were performed at room temperature using an MultiClamp 700B amplifier (Molecular devices). Data were digitized using a Axon DigiData 1440A Data Acquisition System. During electrophysiological recordings, membrane potential was held at − 70 mV. Cells were kept in extracellular solution containing (in mM): 142 NaCl, 8.09 KCl, 6 $MgCl_2$, 1 $CaCl_2$, 10 glucose, 10 HEPES and a final pH of 7.3–7.4. Patch pipettes were pulled from borosilicate glass (Science products) using a Sutter P97 Puller (Sutter Instruments Company). Their resistance ranged from 3 to 5 MΩ. Patch pipettes were filled with intracellular solution containing (in mM): 5 KCl, 4 ATP-Mg, 10 phosphocreatine, 0.3 GTP-Na, 10 HEPES, 125 K-gluconate, 2 MgCl2, 10 EGTA with a final pH of 7.2 and an osmolariy of 290 mosmol. A series of hyperpolarizing and depolarizing step currents were injected to measure intrinsic properties and to elicit action potentials (APs). Whole-cell current-clamp recordings were performed with the internal solution containing (in mM): 125 K-gluconate, 10 KCl, 10 HEPES, 0.5 EGTA, 3 Na_2ATP, 0.5 Na_2GTP, 12 phosphocreatine, pH 7.25, 280 mOsm. Cells were perfused with ACSF, and membrane potentials were kept at − 55 to − 65 mV. The sampling rate was 50 kHz and data were low-pass filtered at 10 kHz. Series resistance (< 20 MΩ) was monitored during the experiment. Cells showing unstable series resistance or resting membrane potential were discarded.

Immunofluorescence and Western blotting analysis

Immunofluorescence (IF): Cells were fixed with 4% PFA for 30 min and blocked with blocking buffer (PBS with 0.05% TritonX-100, 2% bovin serum albumen, and 1% sodium azide) for 1 h. Cells were then stained with primary antibody according to manufacturer's recommendation in blocking buffer overnight at 4 °C. Cells were washed twice with 0.1% PBST and stained with secondary antibody (1:500 in blocking buffer) for 2 h at 25 °C. Cells were washed again with 0.1% PBST and kept in PBS, protected from light. Images were taken on a Zeiss LSM 710 Confocal Microscope.

Western blot (WB): Cells were harvested in Pierce RIPA buffer (Thermo-Fisher Scientific) with 1% protease and 1% phosphatase inhibitors (Thermo-Fisher Scientific) at a density of 10^6 cells/mL. Samples were sonicated for 1 min and centrifuged at full speed for 10 min at 4 °C. Pellets were discarded. Protein concentrations were calculated using Pierce BCA Protein assay (Thermo-Fisher Scientific) and a BioTech plate reader per manufacturer's instructions. 4 × loading buffer (Takara- 9173) was added to each sample and boiled at 100 °C for 5 min. For immunoprecipitation (IP), whole-cell extracts were prepared after transfection or stimulation with appropriate ligands, followed by incubation overnight with appropriate antibodies plus Protein A/G beads (Thermo-Fish Scientific). For IP with anti-Flag or anti-α-Syn antibodies, anti-Flag or anti-α-Syn agarose gels were used. Beads were then washed 5 times with low-salt lysis buffer (50 mM HEPES, 150 mM NaCl, 10% glycerol, 1.5 mM MgCl and 1% TritonX-100), and immunoprecipitates were eluted with 2 × SDS Loading Buffer and resolved by SDS-PAGE. Proteins were transferred to PVDF membranes (Bio-Rad) and further incubated with the appropriate antibodies. Immobilon Western Chemiluminescent HRP Substrate (Millipore) was used for detection.

Quantitative RT-PCR

Total RNA was extracted from cells using the RNeasy Plus Kit (Qiagen) according to the manufacturer's instructions. For RT-PCR analysis, cDNA was generated with High Capacity cDNA Reverse Transcription Kit (Thermo Fisher Scientific) and analyzed by quantitative real-time PCR using the iTaq Universal SYBR Green (Bio-Rad) on a CFX-96 Real-Time PCR Detection System (Bio-Rad). All data were normalized to GAPDH expression mRNA levels.

Construction of plasmids

We used gene cloning and PCR to amplify USP8 cDNA from the human genome, the $USP8^{WT}$ ($USP8^{D442}$) cDNA is amplified from PD3C and the $USP8^{MT}$ ($USP8^{D442G}$) cDNA is amplified from PD3, the primers are described in Table 2. Then, we inserted USP8 ($USP8^{D442}$ or $USP8^{D442G}$) cDNAs downstream of the CMV promoter of pLenti (pLenti-CMV-GFP-Puro, addgene-17448) after digestion with restriction enzyme *Xba*I (NEB-R0145L) and *Sal*I (NEB-R3138L), and verified sequence by sequencing. Later, we added the Flag sequence to the N-terminus of $USP8^{D442}$ and $USP8^{D442G}$ cDNAs or pLenti-empty vector plasmid with restriction enzyme *Xba*I and *Sal*I. For the construction of α-Syn overexpressing plasmid, we used the same gene cloning method to amplify the SNCA (α-Synuclein) DNA by RT-PCR (the primers are showed in Table 2) which was inserted downstream of the CMV promoter of pcDNA3.1 (pcDNA3.1 + , addgene V790-20) after digestion with restriction enzyme *Xba*I (NEB-R0145L) and *Hind*III (NEB-R3104L). All plasmid constructs were sequenced to verify correct sequence with the human CMV

Table 2 Primer list for plasmids constructed

Primers for plasmid construction (F: Forward (5′ to 3′), R: Reverse (5′ to 3′))	
USP8-Cloning-F	GAGCTCTAGAATGCCTGCTGTGGCTTCA
USP8-Cloning-R	ACGCGTCGACTTATGTGGCTACATCAGTTACTCG
USP8-XbaI-Flag-F	GAGCTCTAGAatggactacaaggatgacgatgacaagggaATGCCTGCTGTGGCTTCA
USP8-SalI-R	GACCGTCGACTTATGTGGCTACATCAGTTACTC
plenti-Flag-XbaI-F	GAGCTCTAGAATGGACTACAAGGATGACGATGACAAGGGA
plenti-Flag-SalI-R	GACCGTCGACCTATCCCTTGTCATCGTCATCCTTGTAGTC
SNCA-HindIII-F	GAGCAAGCTTATGGATGTATTCATGAAAGGACTT
SNCA-XbaI-R	GACCTCTAGATTAGGCTTCAGGTTCGTAGT

universal primer. The HA-Ub (pRK5-HA-Ubiquitin-WT, addgene-17608), HA-K63 (pRK5-HA-Ubiquitin-K63, addgene-17606) and the HA-K48 (pRK5-HA-Ubiquitin-K48, addgene-17605) plasmids were kindly provided by Prof. Jun Cui of School of Life Sciences in Sun Yat-sen University.

Cell culture and transfection

Fibroblast and HEK-293T cells were maintained at 37 °C and 5% CO_2 in DMEM containing 10% (vol/vol) FBS (Gibco) and 1% (vol/vol) penicillin–streptomycin (Life Technologies). The method of using Y4 plasmids to reprogram iPSC from fibroblasts had been described previously.

For the transfection of NSCs, we used the lentivirus infection to introduce the $USP8^{D442}$-expressing,$USP8^{D442G}$-expressing or empty (EV) pLenti plasmids into the NSC cells, which were selected with puromycin. The plasmid was co-transfected with psPAX2 and pMD2.G plasmids (Addgene) into HEK-293T cells. 48 h after transfection, the supernatant was collected and virus enriched with Lenti-X concentrator (Clontech). NSCs were transduced with $USP8^{D442}$, $USP8^{D442G}$ or EV lentivirus and selected with 0.5 μg/mL puromycin to generate USP8 ($USP8^{D442}$ or $USP8^{D442G}$) overexpressing NSC cell lines.

For the overexpression of Flag-$USP8^{D442}$, $USP8^{D442G}$, α-Syn and HA-Ub/K63/K48 in HEK-293T cells, Lipofectamine 3000 (Life Technologies) was used to transfected Flag-$USP8^{D442}$, Flag-$USP8^{D442G}$, α-Syn, HA-Ub, HA-K63 or HA-K48 into the HEK-293T cells. 36 h after transfection, cells were harvested in Pierce RIPA buffer to obtain protein extract for the Western Blot analysis.

CRISPR/Cas9-mediated knock-in of D442G mutation into the endogenous gene of hESCs

We designed several gRNAs of 300–500 bp from the mutation site and ligated it with Cas9-P2A (addgene, #99248) plasmid. After using *T7E1* enzyme to verify the cutting efficiency of gRNA, we selected the gRNA with the best cutting efficiency in the follow-up experiment and designed the repair template (the gRNA sequence was GTTGAC ATGGTCTTAGCCTGTGG). We used the DNA of PD patients with $USP8^{D442G}$ mutation as a template to perform PCR, and amplify the uparm fragment (1302 bp) containing the mutation site. Similarly, we use PCR to amplify the downarm (567 bp) of the repair template using the PD patient's genomic DNA. Related PCR primers are shown in Table 3. We first used NotI and EcoRI to double-cut the pBluescriptKS (addgene, #104475), which was run on 1% EB gel and extracted. At the time double-cut the uparm using *Not*I and *EcoR*I and connected uparm and pBluescriptKS with T4 ligase, named uparm-pBluescriptKS. and then double-cut the uparm-pBluescriptKS and downarm using *XhoI* and *KpnI* and connected them with T4 ligase, In this way, the repair template is successfully constructed. We transfected H9 cells with gRNA-Cas9-P2A and Template at a molar ratio of 1:3. Regarding the transfection method of hESC cells, we used the LONZA-4D cell nuclear electrotransfection apparatus, and used the P3 Primary Cell 4D-Nucleofector X Kit CB-150 transfection procedure to transfect ESC-H9 cells. We used puromycin to select for the transfected H9 cells, and then picked single clone, we used the genomic DNA of pick single clone as the template for PCR to detect the existence of uparm, downarm and Puro, inferring the success of homology repair. Then, by transfecting the Cre/Lox (pDZ416 loxP-Kan-loxP, addgene #45163) plasmid to remove the fragments of Loxp-puro-loxp, and verified the deletion by sanger sequencing, we

Table 3 Primer list for CRISPR/Cas9 gene homology repair related plasmids construction

Primers for CRISPR/Cas9 gene homology repair related plasmids Construction (F: Forward (5′ to 3′), R: Reverse (5′ to 3′))	
USP8-uparm-F	atagcggccgcATGGTCTTAGCCTGTGG (NotI)
USP8-uparm-R	ccggaattcTCAGTACATTCTATCACCC (EcoRI)
USP8-downarm-F	ccgctcgagTCTATCCACATTTGCTC (XhoI)
USP8-downarm-R	cggggtaccCATAACTGTTCTTGGTATTA (KpnI)

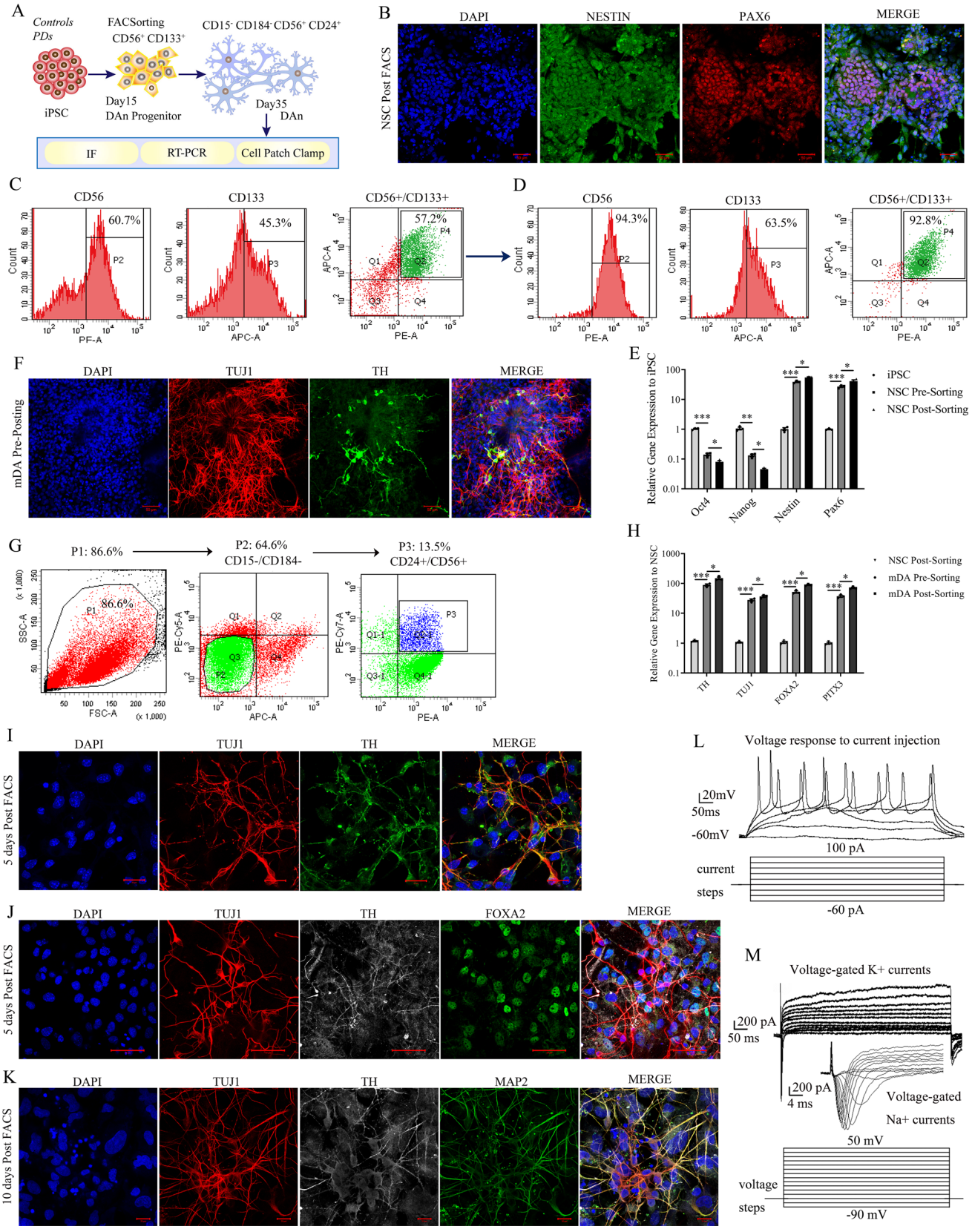
A
Controls
PDs
iPSC
FACSorting
CD56+ CD133+
Day15
DAn Progenitor
CD15- CD184- CD56+ CD24+
Day35
DAn
IF
RT-PCR
Cell Patch Clamp
B
DAPI
NESTIN
PAX6
MERGE
NSC Post FACS
C
CD56
60.7%
CD133
45.3%
CD56+/CD133+
57.2%
D
CD56
94.3%
CD133
63.5%
CD56+/CD133+
92.8%
E
Relative Gene Expression to iPSC
Oct4
Nanog
Nestin
Pax6
iPSC
NSC Pre-Sorting
NSC Post-Sorting
F
mDA Pre-Posting
DAPI
TUJ1
TH
MERGE
G
P1: 86.6%
P2: 64.6%
CD15-/CD184-
P3: 13.5%
CD24+/CD56+
H
Relative Gene Expression to NSC
TH
TUJ1
FOXA2
PITX3
NSC Post-Sorting
mDA Pre-Sorting
mDA Post-Sorting
I
5 days Post FACS
DAPI
TUJ1
TH
MERGE
L
Voltage response to current injection
20mV
50ms
-60mV
100 pA
current
steps
-60 pA
J
5 days Post FACS
DAPI
TUJ1
TH
FOXA2
MERGE
M
Voltage-gated K+ currents
200 pA
50 ms
200 pA
4 ms
Voltage-gated
Na+ currents
50 mV
voltage
steps
-90 mV
K
10 days Post FACS
DAPI
TUJ1
TH
MAP2
MERGE

◂**Fig. 1** Generation and characterization of DAn. **A** Schematic diagram of the process to differentiate hiPSCs into NSCs and DAn. The antibodies used to purify DAn progenitors and DAn are indicated. **B** Immunostaining NSCs for the expression of NESTIN and PAX6 to confirm the NSC identity on day 15 of differentiation. Scale bars, 50 μm. **C**, **D** $CD56^+/CD133^+$ NSCs were enriched by flow cytometric cell sorting. In the shown experiment, the percentage of $CD56^+/CD133^+$ NSCs was 57% before the sorting (**C**) and 92% after the sorting (**D**). **E** qPCR analysis of the expression of various genes in hiPSCs, unsorted NSCs and sorted NSCs. *OCT4* (one-way ANOVA: $F=352.395$, $p<0.001$; post hoc *Dunnett T3* test), *NANOG* (one-way ANOVA: $F=79.930$, $p<0.001$; post hoc *Dunnett T3* test), *Nestin* (one-way ANOVA: $F=176.107$, $p<0.001$; post hoc *Dunnett T3* test), *PAX6* (one-way ANOVA: $F=54.099$, $p<0.001$; post-hoc *LSD* test). $n=3$. $^*p<0.05$, $^{**}p<0.01$, $^{***}p<0.001$. **F** Immunostaining DAn for the expression of TH and TUJ1 to confirm the identity of dopaminergic lineage on days 30 of differentiation. Scale bars, 50 μm. **G** Purification of $CD15^-CD184^-CD24^+CD56^+$ DAn by flow cytometric cell sorting. **H** qPCR analysis of the expression of various genes in sorted NSCs, unsorted DAn and enriched DAn. *TH* (one-way ANOVA: $F=73.188$, $p<0.001$; post-hoc *Dunnett T3* test), *TUJ1* (one-way ANOVA: $F=82.439$, $p<0.001$; post-hoc *LSD* test), *FOXA2* (one-way ANOVA: $F=191.383$, $p<0.001$; post-hoc *LSD* test), *PITX3* (one-way ANOVA: $F=171.304$, $p<0.001$; post-hoc *LSD* test). $n=3$, $^*p<0.05$, $^{***}p<0.001$. **I–K** Immunostaining of purified DAn for the expression of TH, TUJ1, FOXA2 and MAP2 to confirm the dopaminergic lineage. Scale bars, 20 μm (**I**, **K**) and 50 μm (**J**). **L**, **M** DAn fired evoked action potential (**L**) and had voltage-gated K^+ and Na^+ currents (**M**) shown by cell patch clamp electrophysiology

obtained the cells with $H9^{USP8-D442G}$ homozygous and heterozygous mutations, named $H9^{USP8-A/G}$ and $H9^{USP8-G/G}$ respectively.

$USP8^{D442G}$ sequencing validation

The whole-genome sequencing of fibroblast genomic DNA was performed by WuXi Genome Center and bioinformatics analyzed in Cancer Research Institute, School of Basic Medical Sciences, Southern Medical University. We found a genetic locus, $USP8^{D442G}$ (rs:3743044), which was mutated in the two PDs but wild type in the two healthy siblings' controls. We obtained blood samples from PD patients and healthy persons in the Guangdong Provincial Hospital of TCM under the guidance and approval of the Board of Ethics with informed consents. We used the HiPure Blood DNA Mini kit (Magen, D3111-03) to extract DNA from the blood. Then, we used the DNA as a template to perform PCR to get the target DNA fragment for sequencing by BGI Company. The sequencing data were analyzed and compared with BioEdit Sequence Alignment Editor software, and the $USP8^{D442G}$ mutation rate was calculated using Excel.

Quantification and statistical analysis

Data are represented as mean ± SEM unless otherwise indicated, and Student's *T* test was used for comparing two groups. *F*-test was tested for comparing variances. For comparing multiple groups, one-way ANOVA or two-way ANOVA were used. *N* was indicated in figure legend. All statistical analysis was determined with the GraphPad Prism 5 software. Differences between two groups were considered significant when *p* value is less than 0.05 ($^*p<0.05$, $^{**}p<0.01$, $^{***}p<0.001$; n.s., non-significant. Error bars indicate means ± s.d.). $N=3$ indicated three independent parallel experiments.

Results

Generation of integration-free hiPSC lines from PD patients and healthy siblings

To establish hiPSCs from PD patients and healthy siblings, we obtained dermal fibroblasts from five PD patients (named PD1-5), and two from healthy siblings (named PD3C and PD4C). Primary cultures of dermal fibroblasts were reprogrammed to generate 2–8 independent hiPSC lines per individual sample. All hiPSC lines were thoroughly characterized and shown to be fully reprogrammed to pluripotency, as judged by colony morphology, alkaline phosphatase (ALP) staining (Fig. S1A), pluripotency-specific surface markers (OCT4 and TRA1-81) (Fig. S1B), and expression of pluripotency factors (*OCT4*, *SOX2*, and *NANOG*) (Fig. S1C). Most of the hiPSC lines were free of the genomic integration of the vector (Fig. S1D). In *vitro* embryoid body formation assay and in vivo teratomas formation assay indicated that hiPSCs could differentiate into each of the three germ layers, confirming the pluripotency of these hiPSC lines (Fig. S1E). Here, we displayed the pluripotency data of two cloned iPSCs from four samples: PD3C, PD3, PD4C and PD4. Through cell morphology observation and immunofluorescence analysis of TRA-1-81, OCT4 and SSEA4 (Fig. S2A), and the detection of *OCT4* and *NANOG* mRNA expression by qPCR (Fig. S2D, E), it was proven that there was no significant difference between different clones (Fig. S2).

Derivation of DAn neurons from hiPSCs

With some modifications of the neuronal differentiation protocols [15], we differentiated hiPSC into neural stem cells (NSC) and subsequently DAn (Fig. 1A). Using a combination of surface markers specific for iPSCs, NSCs, and neurons, we purified NSCs 12 days after differentiation and DAn 30 days after differentiation. By flow cytometric sorting of $CD56^+CD133^+$ double positive cells, NSCs expressing NESTIN and PAX6 were significantly enriched in the differentiating culture (Fig. 1B–E). By purifying $CD56^+CD24^+CD15^-CD184^-$ cells (Fig. 1F–I), dopaminergic neurons, as identified by the expression of Class III β-Tubulin (TUJ1) and Tyrosine hydroxylase (TH), were

greatly enriched (Fig. 1E, H, I). Consistent with this finding, the expression of DAn-related genes such as TH, TUJ1, FOXA2, and PITX3 was significantly higher in sorted cells than in NSCs and unsorted neurons, indicating an efficient enrichment for DAn population (Fig. 1H–K). Using Patch-Clamp technique, we found that hiPSC-derived DAn could fire action potentials in response to injected current and exhibit voltage-gated sodium as well as potassium currents, supporting the notion that these DAn were functional neurons (Fig. 1L–M). We randomly detected the difference of DAn differentiation between two iPSC clones of four samples: PD3C, PD3, PD4C, and PD4. NSC was detected on the 15th day of differentiation, and DAn was detected on the 30th. The results showed that different clones could normally differentiate into NSC (Fig S2B) and DAn (Fig S2C), and there was no significant difference in the proportion of NESTIN/PAX6 (Fig S2F) and TH/TUJ1 (Fig S2G) double-positive cells. There was no significant difference in the specific gene expression of NSC (Fig S2H, I) and DAn (Fig S2J–M) from different clones. However, it could be observed from WB data that there was a phenotype of abnormal accumulation of α-Syn in DAns from PD (Fig S2N, O).

α-Syn accumulation in PD hiPSC-derived DAn

A hallmark of PD pathology is the accumulation of α-Syn in their DAn [16]. Therefore, we examined the expression of α-Syn in the DAn derived from PD and control hiPSCs. The immunofluorescence (IF) analysis showed higher levels of α-Syn in PD DAn than control DAn (Fig. 2A, B). In support of this finding, western blotting analysis confirmed that the protein levels of α-Syn in PD DAn were higher than those in control DAn (Fig. 2G–J). In addition, we observed that the subcellular localization of α-Syn was different between PD and control DAn. In the control DAn, α-Syn was mainly localized in dendrites. But in the PD DAn, α-Syn was mainly localized in the cytoplasmic soma (Fig. 2A, B). According to the previously reported method [14], we quantified the localization of the soma and dendrites of α-Syn in DAn cells. The results show that compared with Ctrl, the α-Syn of DAns derived from PD iPSCs is more concentrated in the cytoplasm and less distributed in the dendrites (Fig. 2C–F).

USP8^{D442G} polymorphism is associated with PD

To understand the genetic basis of PD, we performed whole-genome DNA sequencing of the fibroblasts from PD patients and healthy siblings, and identified USP8 that harbored a polymorphic D442G site (dbSNP: rs3743044) in both PD patients but not in their healthy siblings (Fig. 3A). Based on our analysis of 218 healthy Chinese controls as well as the data from existing genomic databases, the incidence of D442G polymorphism in the general population is about 9.2%, but 19.8% in the 106 PD patients we analyzed. Through Chi-Square Calculator statistical, p value = 0.00689 ($p < 0.05$), suggesting that the incidence of USP8 D442G in PD patients is significantly higher than that in healthy people. In addition, the incidence of USP8^{D442G} in the age groups of 30–50, 51–60, 61–70 and 71–80 was 38.1% (8/21), 33.3% (7/21), 23.8% (5/21) and 4.8% (1/21), respectively, suggesting that USP8^{D442G} polymorphism is associated with the early-onset Chinese PD patients (Fig. 3B). The frequency of USP8^{D442G} polymorphism is also low in the general population worldwide (Fig. 3C). We examined the frequency of USP8^{D442G} allele in 10,000 human genomes [17], ExAC database [18] and Han90 [19], as shown in Table 4. The frequency of rs3743044 in 10,000 human genome is less than 3%, and that in Han90 is 11.1%. Using PredictProtein software to study the structure and function of USP8 in the PDB database [20, 21], it was predicted that this polymorphism could induce the structural and functional change of USP8 (Fig. 3D). In this context, the harmful score of D replaced by G is the biggest among the 19 amino acids.

USP8^{D442G} promotes α-Syn accumulation in DAn

Previous studies have implicated USP8 in the deubiquitination of α-Syn and thus inhibits its degradation by lysosome [10]. To study the effects of USP8^{D442G} polymorphism on the stability of α-Syn in DAn, we used lentivirus to overexpress USP8^{D442} or USP8^{D442G} in NSCs derived from PD3C, PD3, PD4C and PD4 hiPSCs (Fig. S3A-G). The expression of USP8^{D442D} or USP8^{D442G} did not affect the expression of NESTIN in NSCs, suggesting that their expression in the NSCs did not affect the status of NSCs (Fig. S3H).

While the expression of both USP8^{D442} and USP8^{D442G} increased α-Syn accumulation in the control hiPSC-derived DAn, the overexpression of USP8^{D442G} but not USP8^{D442} in PD hiPSC-derived DAn could further increase α-Syn accumulation (Fig. 4A, D, G, H). In PD3C and PD4C DAn, α-Syn was detected mostly in non-accumulated protein cluster distributed in dendrites; While in PD3 and PD4 DAn with or without overexpressing USP8^{D442G}, α-Syn was detected mostly in accumulated protein cluster distributed in the cytoplasm (Fig. 4A–F). In addition, the shape and distribution of α-Syn in PD3 and PD4 DAn could be partially reversed by the overexpression of USP8^{D442} (Fig. 4A–F). These findings further

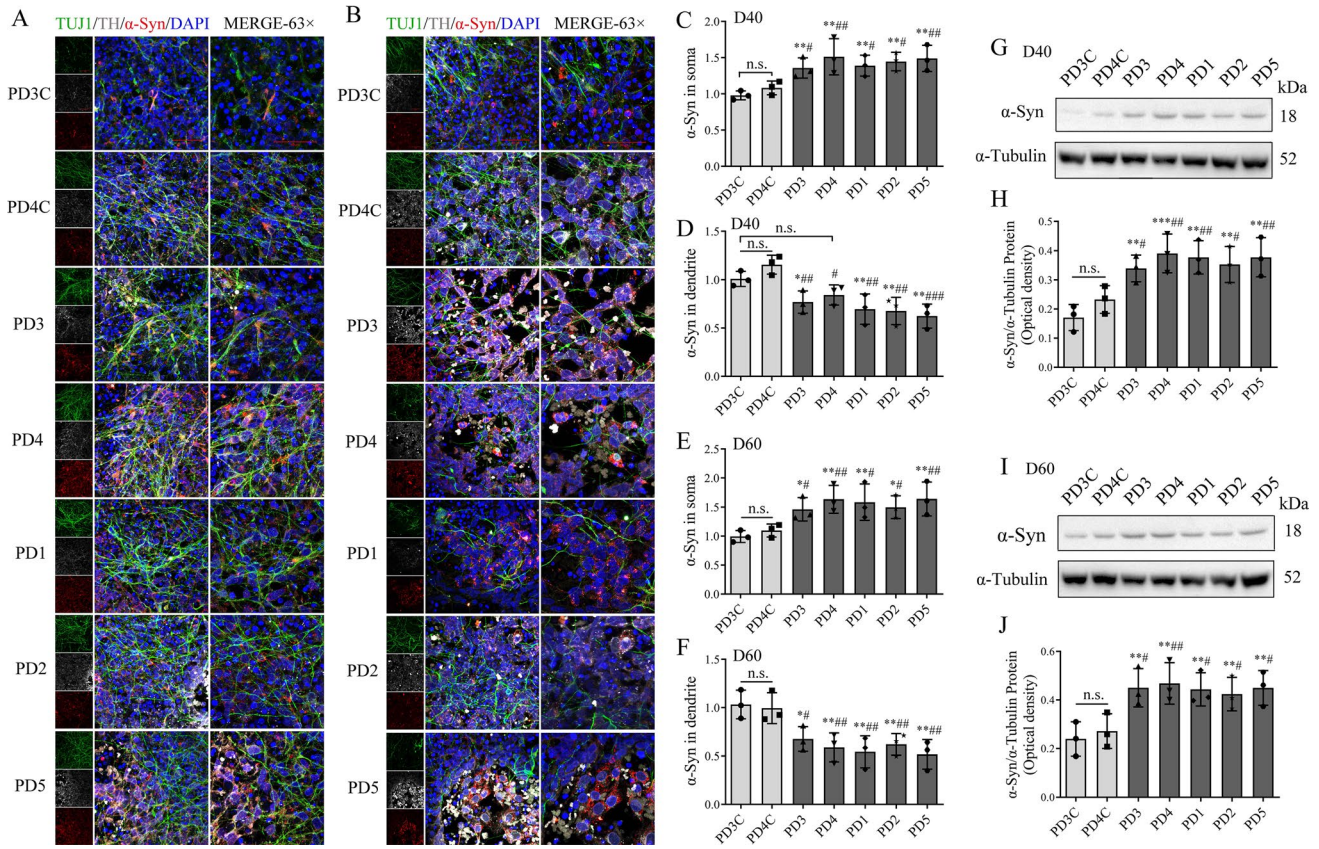

Fig. 2 α-synuclein is accumulated in DAn derived from PD hiPSCs. **A**, **B** Immunostaining of DAn derived from control and PD hiPSCs on day 40 (**A**) and day 60 (**B**) after the onset of differentiation for the expression of TUJ1 (green), TH (gray), α-Syn (red), nuclei counterstained with DAPI (blue). Scale bars, 50 μm. The quantitative data of the expression of α-Syn in the cytoplasm soma (**C**) and nerve dendrite (**D**) at day 40 of differentiation. In **C**, one-way ANOVA: $F=5.532$, $p=0.004$; post-hoc *LSD* test. In **D**, one-way ANOVA: $F=7.985$, $p=0.001$; post-hoc *LSD* test. $n=3$. When compared to PD3C, p values are indicated with *, $^{*}p<0.05$, $^{**}p<0.01$; When compared to PD4C, p values are indicated with $^{\#}$, $^{\#}p<0.05$, $^{\#\#}p<0.01$, $^{\#\#\#}p<0.001$; n.s., non-significant. The quantitative data of the expression of α-Syn in the cytoplasm soma (**E**) and nerve dendrite (**F**) at days 60 of differentiation. In **E**, one-way ANOVA: $F=4.401$, $p=0.011$; post-hoc *LSD* test. In **F**, one-way ANOVA: $F=6.430$, $p=0.002$; post-hoc *LSD* test. $n=3$. When compared to PD3C, p values are indicated with *, $^{*}p<0.05$, $^{**}p<0.01$; When compared to PD4C, p values are indicated with $^{\#}$, $^{\#}p<0.05$, $^{\#\#}p<0.01$, $^{\#\#\#}p<0.001$; n.s., non-significant. The protein levels of α-Syn in DAn derived from control and PD hiPSCs on day 40 (**G**, **H**) or day 60 (**I**, **J**) after the onset of differentiation. The protein levels of α-Syn were normalized with protein levels of α-Tubulin. **G**, **I** The representative Western blot data are shown. **H**, **J** Statistical analysis of the relative expression levels of α-Syn are shown. In **H**, one-way ANOVA: $F=6.735$, $p=0.002$; post-hoc *LSD* test. In **J**, one-way ANOVA: $F=4.937$, $p=0.007$; post-hoc *LSD* test. $n=3$. When compared to PD3C, p values are indicated with *, $^{*}p<0.05$, $^{**}p<0.01$, $^{***}p<0.001$; When compared to PD4C, p values are indicated with $^{\#}$, $^{\#}p<0.05$, $^{\#\#}p<0.01$; n.s., non-significant. The genotype of PD3C, PD4C, PD1, and PD2 hiPSC lines is $USP8^{D442}$, while the genotype of PD3, PD4, and PD5 hiPSC lines is $USP8^{D442G/D442}$. Data are based on three independent differentiation experiments of one hiPSC clone per patient

support the notion that $USP8^{D442G}$ contributes to abnormal accumulation of α-Syn in DAn.

DAn derived from hESCs harboring $USP8^{D442G}$ knock-in allele exhibited abnormal α-Syn accumulation and subcellular localization

To further confirm that D442G polymorphism directly contributes to PD-related pathogenesis, we used CRISPR/CAS9 technology to introduce the D442G mutation into the endogenous USP8 gene of H9 hESCs, obtaining both heterozygous $H9^{USP8-A/G}$ and homozygous $H9^{USP8-G/G}$ hESC cell lines. $H9^{WT}$, $H9^{USP8-A/G}$ and $H9^{USP8-G/G}$ hESCs all showed normal hESC phenotypes (Fig. 5A, B). There was no significant difference in the NSCs differentiated from $H9^{WT}$, $H9^{USP8-D/G}$ and $H9^{USP8-G/G}$ hESCs, such as the co-expression of PAX6 and NESTIN (Fig. 5C, D). However, when NSCs were further differentiated into DAn, the $H9^{USP8-D/G}$ hESC-derived

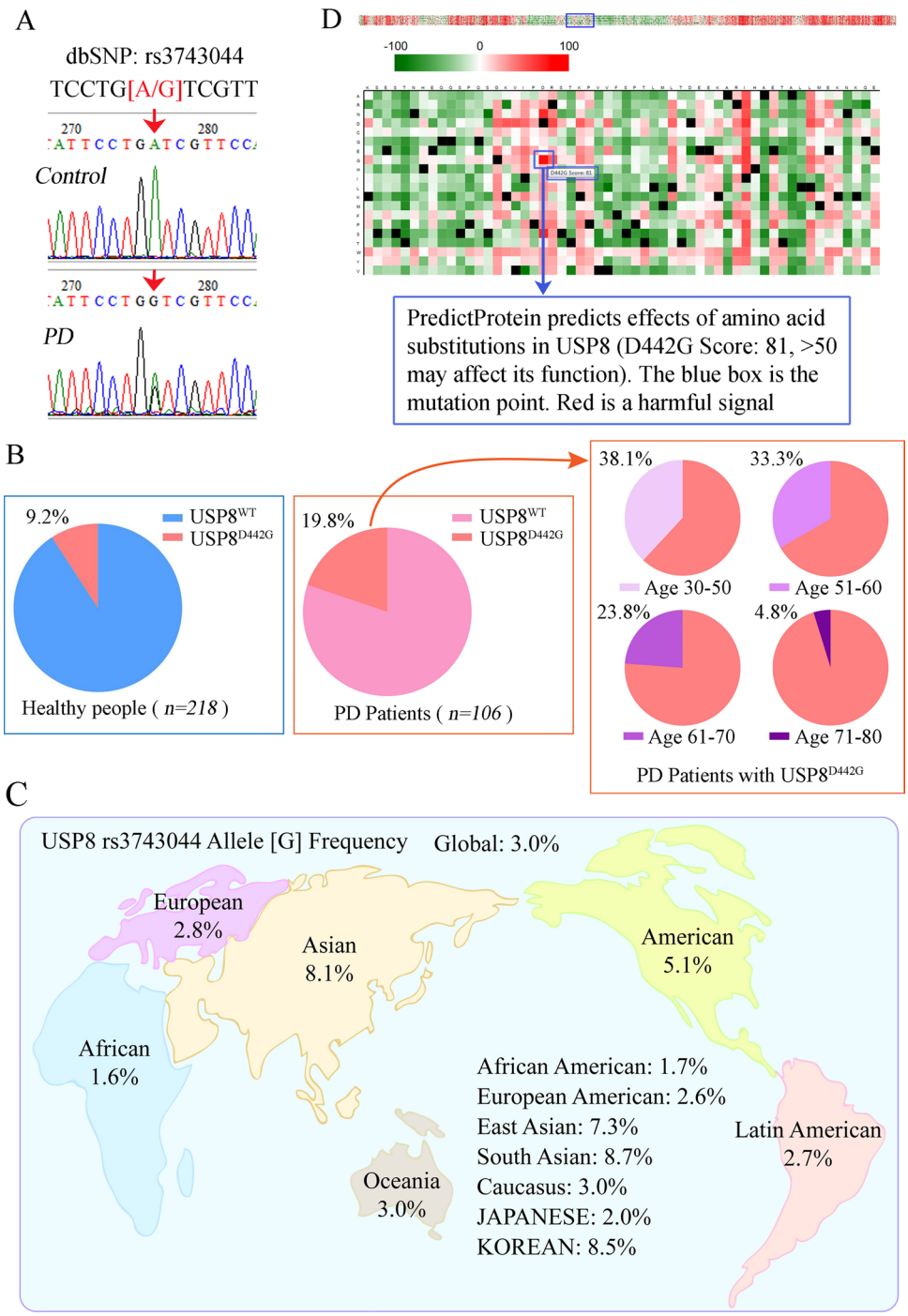

Fig. 3 USP8^{D442G} polymorphism is associated with PD. **A** Sequencing data show heterozygous USP8^{D442G} polymorphism in a PD patient. **B** Pie chart shows the frequency of USP8^{D442G} polymorphism in 218 healthy Chinese individuals and the 106 PD patients. The frequencies of USP8^{D442G} polymorphism in different age groups are shown (right). **C** The frequencies of USP8^{D442G} polymorphism worldwide based on data from National Library of Medicine database. **D** Protein predicts the effects of amino acid substitutions at D442 in USP8 (D442G, Score: 81). The score over 50 may affect its function. The blue box is the SNP site, red indicates the highest harmful coefficient

Table 4 Occurrence frequency of rs3743044 in ten thousand genomes, ExAC and Han90

ID	ExAC	ExAC-EAS	10K	EUR	AFR	EAS	CSA	ADMIX	Han90
rs3743044	0.0362	0.0767	0.027	0.029	0.021	0.093	0.046	0.022	0.111

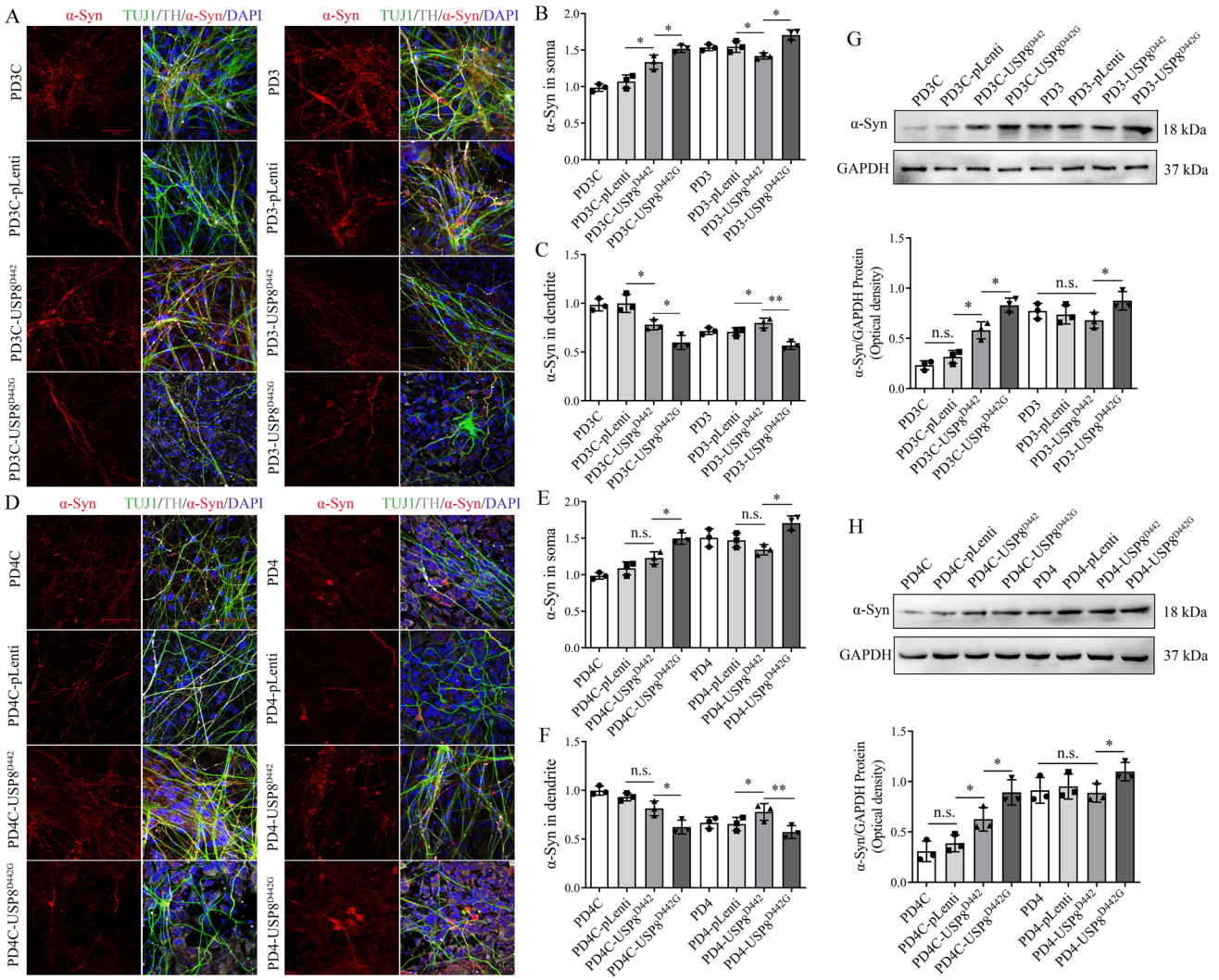

Fig. 4 USP8^{D442G} promotes α-Syn accumulation in DAn. **A**, **D** Immunostaining for α-Syn (red), TUJ1 (green), and TH (gray) in DAn derived from PD3C/PD3 (**A**) and PD4C/PD4 (**D**) hiPSCs transduced with empty lentiviral vector or lentivirus expressing USP8^{D442G} or USP8^{D442}. Nuclei were counterstained with DAPI (blue). Scale bars, 50 µm. **B**, C, **E**, **F** The subcellular localization of α-Syn in DAn derived from PD3C/PD3 hiPSCs (**B**, **C**) or PD4C/PD4 hiPSCs (**E**, **F**) transduced with empty lentiviral vector or lentivirus expressing USP8^{D442G} or USP8^{D442}. The proportion of accumulated α-Syn in soma and non-accumulated α-Syn in dendrite in DAn derived from PD3C/PD3 hiPSCs (**B**, **C**) or PD4C/PD4 hiPSCs (**E**, **F**) was statistically analyzed to quantify the pathological changed of α-Syn. (**B**, two-way ANOVA: $F=23.416$, $p<0.000$; Tukey's post-hoc test. **C**, two-way ANOVA: $F=13.579$, $p<0.000$; Tukey's post-hoc test. **E**, two-way ANOVA: $F=19.731$, $p<0.000$; Tukey's post-hoc test. **F**, two-way ANOVA: $F=11.971$, $p<0.000$; Tukey's post-hoc test). $n=3$, $^{*}p<0.05$, $^{**}p<0.01$, non-significant, non-significant. **G, H** The protein levels of α-Syn in various hiPSC-DAn. DAn derived from PD3C/PD3 hiPSCs (**G**) or PD4C/PD4 hiPSCs (**H**) were transduced with empty lentivirus or lentivirus expressing USP8^{D442G} or USP8^{D442}. Quantification of the relative protein levels of α-Syn normalized to GAPDH in various hiPSC-DAn as shown in (**G**) and (**H**) ($n=3$, $^{*}p<0.05$, $^{**}p<0.005$; n.s., non-significant. **G**, two-way ANOVA: $F=20.109$, $p<0.000$; Tukey's post-hoc test. **H**, two-way ANOVA: $F=9.816$, $p<0.000$; Tukey's post hoc test). Data are based on one clone per patient line differentiated three times

DAn showed abnormal accumulation and localization of α-Syn, which was worsen in DAn derived from homozygous H9$^{USP8-G/G}$ hESC (Fig. 5E–G). We randomly selected three clones from each ESC-H9 cell line for comparative study, and obtained similar results (Fig. S4). These results demonstrate that USP8^{D442G} polymorphism directly contributes to the abnormal accumulation of α-Syn.

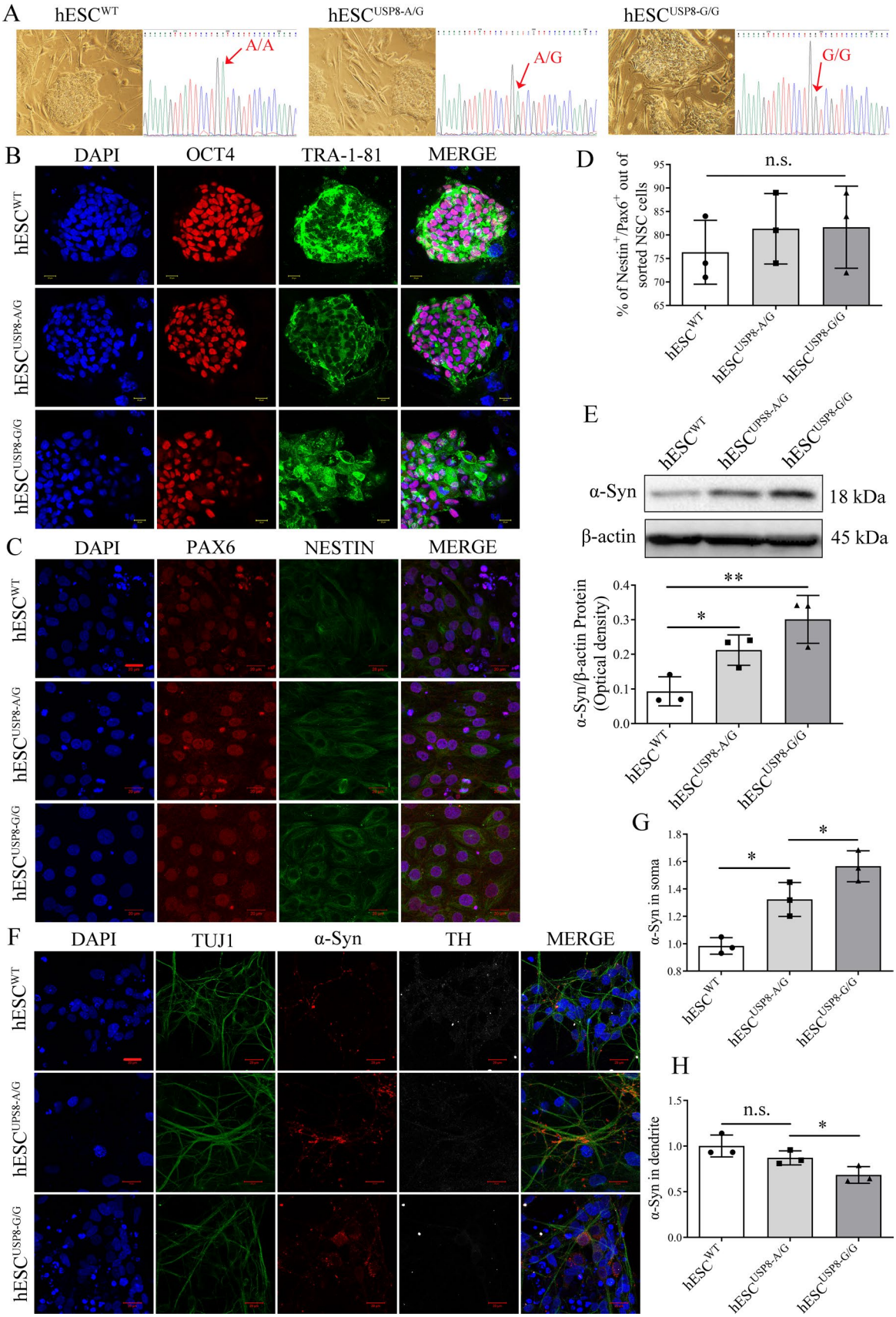
A
hESCWT
hESCUSP8-A/G
hESCUSP8-G/G
A/A
A/G
G/G
B
DAPI
OCT4
TRA-1-81
MERGE
C
DAPI
PAX6
NESTIN
MERGE
D
n.s.
% of Nestin+/Pax6+ out of sorted NSC cells
E
α-Syn
β-actin
18 kDa
45 kDa
α-Syn/β-actin Protein (Optical density)
F
DAPI
TUJ1
α-Syn
TH
MERGE
G
α-Syn in soma
H
n.s.
α-Syn in dendrite

◂**Fig. 5** DAn derived from hESCs harboring $USP8^{D442G}$ knock-in allele exhibited α-Syn accumulation and subcellular localization. **A** Knock-in D442G SNP into the endogenous USP8 gene of hESCs. Sequencing results indicate the successful generation of heterozygous $H9^{USP8-A/G}$ and homozygous $H9^{USP8-G/G}$ hESCs. **B** hESC, $hESC^{USP8-A/G}$ and $hESC^{USP8-G/G}$ co-express pluripotency markers OCT4 and TRA-1-81 proteins as shown by immunofluorescence analysis. Scale bars, 20 µm. **C**, **D** The co-expression of PAX6 and NESTIN proteins in NSCs derived from hESC, $hESC^{USP8-A/G}$ and $hESC^{USP8-G/G}$ was revealed by immunostaining (**C**) and statistical analysis (**D**). One-way ANOVA: $F=0.449$, $p=0.658$, $n=3$, n.s., non-significant. Scale bars, 20 µm. **E** The relative protein levels of α-Syn in DAn derived from hESC, $hESC^{USP8-A/G}$ and $hESC^{USP8-G/G}$. One-way ANOVA: $F=11.555$, $p=0.009$; post-hoc *LSD* test, $n=3$. $^{*}p<0.05$, $^{**}p<0.01$. **F** Immunostaining for α-Syn (red), TUJ1 (green), and TH (gray) in DAn derived from hESC, $hESC^{USP8-A/G}$ and $hESC^{USP8-G/G}$. Nuclei were counterstained with DAPI (blue). Scale bars, 20 µm. **G**, **H** The subcellular localization of α-Syn in DAn derived from hESC, $hESC^{USP8-A/G}$ and $hESC^{USP8-G/G}$. The proportion of non-accumulated protein cluster in synapse and accumulated in soma was statistically analyzed to quantify the abnormal accumulation of α-Syn (**G**, one-way ANOVA: $F=24.271$, $p=0.001$; post-hoc *LSD* test. **H**, one-way ANOVA: $F=7.958$, $p=0.021$; post-hoc *LSD* test). $n=3$, $^{*}p<0.05$, n.s., non-significant

D442G polymorphism promotes the interaction between USP8 and α-Syn, enhancing the deubiquitination of α-Syn

USP8 can remove the K63-linked ubiquitin chains on α-Syn that reduces its lysosomal degradation in dopaminergic neurons and may contribute to α-Syn accumulation [10]. To elucidate the mechanism how $USP8^{D442G}$ polymorphism contributes to the abnormal accumulation of α-Syn, we examined the impact of D442G on the interaction between USP8 and α-Syn. Using CO-immunoprecipitation (Co-IP) assay, we showed that D442G polymorphism increases the interaction between USP8 and α-Syn (Fig. 6A, B). In addition, $USP8^{D442G}$ could deubiquitinate α-Syn more efficiently than $USP8^{D442}$, leading to abnormal α-Syn accumulation (Fig. 6C, D). Therefore, D442G polymorphism is pathogenic for PD.

Discussion

α-Syn is an abundant neuronal protein mainly located at the presynaptic terminal and its accumulation closely related to Parkinson's disease genetically and pathologically. α-Syn has a unique structure with its C-terminus highly acidic and most of it unstructured [22]. α-Syn is a target for multiple post-translational modifications, acetylation [23], sumoylation [24], glycosylation [25], proteolysis [26], and ubiquitination [27], which modulate its interaction with proteins including self-aggregation [28]. Presynaptic localization of α-Syn suggests synaptic-related regulatory functions that maintain neurons during intense neuronal activity [29].

Aggregation of α-Syn in neurons is believed to be toxic and causes its accumulation [10], and even propagate between neurons [30]. Genetic factors, including point mutations and gene rearrangements, are the key factors that cause α-Syn aggregation. For example, α-Syn mutations, such as A53T, A30P, E46K, or SNCA triplications, can often lead to early onset PD [31–33]. Recent studies have revealed α-Syn is mainly undergoing ubiquitin-dependent lysosomal degradation [34]. In this context, previous findings implicate ubiquitin-specific proteases (USPs), which regulate the ubiquitination levels of proteins, in neurodegeneration [35, 36]. For example, USP13 can regulates α-Syn ubiquitination in models of α-Synucleinopathies [9]. USP14 and OTUB1 have been reported to regulate tau-deubiquitination and control its clearance via the proteasome [7, 37]. USP8 could remove K63-linked ubiquitin chains on α-Syn and reduce its lysosomal degradation in DAn, leading to α-Syn accumulation [10].

Conclusions

While the phenotypic defects such as the accumulation and aggregation of α-Synuclein is common among PD patients, the mechanisms driving such defects could be many. We discovered that a USP8 polymorphism, USP8D442G associated with early-onset Chinese PD patients, contributes to the abnormal accumulation and subcellular localization of α-Synuclein. It will be important to screen the PD patients worldwide to determine whether this polymorphism is involved in non-Chinese PD patients. The expression of $USP8^{D442G}$ in DAn can lead to abnormal subcellular localization and accumulation of α-Syn. Mechanistically, this polymorphism increased the interaction between USP8 and α-Syn and the deubiquitination of α-Syn, leading to an inhibition of lysosome-mediated degradation of α-Syn and its accumulation. This will contribute to the pathogenesis of PD. Our data also show that this polymorphism could induce the abnormal localization of the accumulated α-Syn in the cytoplasm of DAn, suggesting that D442G might change the structure of USP8 and its interaction with other proteins, modulate the subcellular localization of α-Syn. Therefore, our findings reveal new mechanisms into the genetic basis of PD pathogenesis and provide potential therapeutic and diagnostic targets for PD.

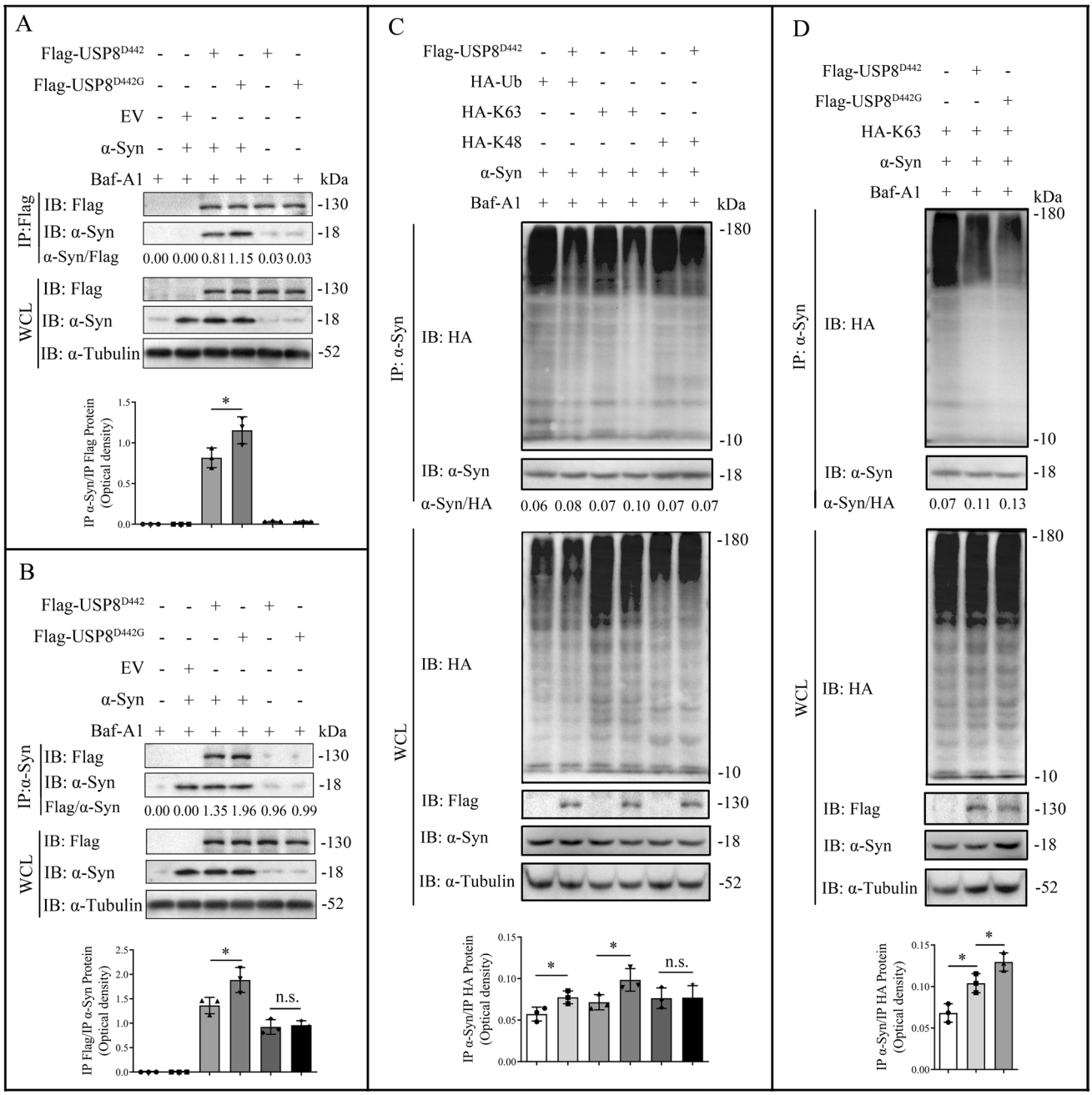

Fig. 6 D442G polymorphism promotes the interaction between USP8 and α-Syn, enhancing the deubiquitination of α-Syn. **A** Co-immunoprecipitation analysis of Flag-tagged USP8^{D442} or USP8^{D442G} and co-expressed α-Syn in 293T cells. The IP α-Syn/IP Flag of USP8^{D442G} was significantly higher than that of USP8^{D442} ($n=3$, $^{*}p<0.05$, according to independent samples *t*-test), suggesting that the combination of USP8^{D442G} and α-Syn was enhanced. **B** Co-IP analysis of the interaction between USP8^{D442} or USP8^{D442G} and α-Syn. α-Syn was immunoprecipitated from 293T cells overexpressing USP8^{D442} or USP8^{D442G} and α-Syn, and the levels of indicated proteins in the immunoprecipitated were analyzed. The IP Flag/IP α-Syn of USP8^{D442G} was significantly higher than that of USP8^{D442} ($n=3$, $^{*}p<0.05$, according to independent samples *t*-test). It is proved again that USP8^{D442G} has stronger combining ability with α-Syn than USP8^{D442}. **C** The ubiquitination levels of α-Syn in cells expressing USP8. α-Syn was immunoprecipitated from 293T cells expressing α-Syn, HA-Ub, and HA-K63 or HA-K48 single-lysine ubiquitin and its ubiquitination determined with anti-HA antibody. The statistical results showed that USP8^{D442} could significantly clear K63 ubiquitin chain ($n=3$, $^{*}p<0.05$, according to independent samples *t*-test), but was insensitive to K48 ubiquitin chain (n.s., non-significant, according to independent samples *t*-test). **D** The de-ubiquitination of K63-linked ubiquitin chain on α-Syn in 293 cells expressing USP8^{D442} or USP8^{D442G} and α-Syn. The quantitative results showed that USP8^{D442G} was more capable of scavenging K63 ubiquitin chain than USP8^{D442} ($n=3$, $^{*}p<0.05$, according to independent samples *t*-test)

Supplementary Information The online version contains supplementary material available at https://doi.org/10.1007/s00018-023-05006-0.

Acknowledgements We thank Dr. X. Luo for collecting cells from PD patients and healthy siblings, Drs. Z. Huang and J. Wang for helping the analysis of sequencing data.

Author contributions YX conceptualized, designed, and supervised the research; SW and TL conducted the experiments.; YX, SW analyzed the data; YX and SW wrote the manuscript. All authors revised and approved the manuscript.

Funding This work was supported by the National Natural Science Foundation of China (Nos. 81930084, U1601222), National Key Research and Development Program of China (2022YFC3401600), the Fundamental Research Funds for the Central Universities (No. 2021FZZX001-42), Ministry of Science and Technology of China (2103ZX10002008002), the Key Research and Development Program of Guangdong Province (2019B020235003), Department of Science and Technology of Guangdong Province (2020A1515110450), Traditional Chinese Medicine Bureau Of Guangdong Province of China (20211183, 20225009), the Special Project of State Key Laboratory of Dampness Syndrome of Chinese Medicine (SZ2021KF15) and the Specific Research Fund for TCM Science and Technology of Guangdong Provincial Hospital of Chinese Medicine (YN2015QN04 and 2020KT1079).

Availability of data and materials The published article includes all datasets generated or analyzed during this study. The whole-genome sequencing data can be accessed from Genome Sequence Archive (https://ngdc.cncb.ac.cn/gsa, accession number: HRA002315). All datasets supporting this study are available from the lead contact, Dr. Yang Xu (xuyang2020@zju.edu.cn) upon request.

Declarations

Conflict of interest The authors declare no competing interests.

Ethics approval and consent to participate The study was approved by the Guangdong Provincial Hospital of Traditional Chinese Medicine (TCM) Board of Ethics.

Consent for publication Not applicable.

References

1. Kalia LV, Lang AE (2015) Parkinson's disease. Lancet 386:896–912. https://doi.org/10.1016/S0140-6736(14)61393-3
2. Kikuchi T, Morizane A, Doi D, Magotani H, Onoe H, Hayashi T, Mizuma H, Takara S, Takahashi R, Inoue H, Morita S, Yamamoto M, Okita K, Nakagawa M, Parmar M, Takahashi J (2017) Human iPS cell-derived dopaminergic neurons function in a primate Parkinson's disease model. Nature 548:592–596. https://doi.org/10.1038/nature23664
3. Lonskaya I, Hebron ML, Desforges NM, Schachter JB, Moussa CE (2014) Nilotinib-induced autophagic changes increase endogenous parkin level and ubiquitination, leading to amyloid clearance. J Mol Med (Berl) 92:373–386. https://doi.org/10.1007/s00109-013-1112-3
4. Zheng N, Shabek N (2017) Ubiquitin ligases: structure, function, and regulation. Annu Rev Biochem 86:129–157. https://doi.org/10.1146/annurev-biochem-060815-014922
5. Yau RG, Doerner K, Castellanos ER, Haakonsen DL, Werner A, Wang N, Yang XW, Martinez-Martin N, Matsumoto ML, Dixit VM, Rape M (2017) Assembly and function of heterotypic ubiquitin chains in cell-cycle and protein quality control. Cell 171(918–933):e20. https://doi.org/10.1016/j.cell.2017.09.040
6. Schmidt MF, Gan ZY, Komander D, Dewson G (2021) Ubiquitin signalling in neurodegeneration: mechanisms and therapeutic opportunities. Cell Death Differ 28:570–590. https://doi.org/10.1038/s41418-020-00706-7
7. Lee JH, Shin SK, Jiang Y, Choi WH, Hong C, Kim DE, Lee MJ (2015) Facilitated Tau degradation by USP14 aptamers via enhanced proteasome activity. Sci Rep 5:10757. https://doi.org/10.1038/srep10757
8. Wang P, Joberty G, Buist A, Vanoosthuyse A, Stancu IC, Vasconcelos B, Pierrot N, Faelth-Savitski M, Kienlen-Campard P, Octave JN, Bantscheff M, Drewes G, Moechars D, Dewachter I (2017) Tau interactome mapping based identification of Otub1 as Tau deubiquitinase involved in accumulation of pathological Tau forms in vitro and in vivo. Acta Neuropathol 133:731–749. https://doi.org/10.1007/s00401-016-1663-9
9. Liu X, Hebron M, Shi W, Lonskaya I, Moussa CE (2019) Ubiquitin specific protease-13 independently regulates parkin ubiquitination and alpha-synuclein clearance in alpha-synucleinopathies. Hum Mol Genet 28:548–560. https://doi.org/10.1093/hmg/ddy365
10. Alexopoulou Z, Lang J, Perrett RM, Elschami M, Hurry ME, Kim HT, Mazaraki D, Szabo A, Kessler BM, Goldberg AL, Ansorge O, Fulga TA, Tofaris GK (2016) Deubiquitinase Usp8 regulates alpha-synuclein clearance and modifies its toxicity in Lewy body disease. Proc Natl Acad Sci U S A 113:E4688–E4697. https://doi.org/10.1073/pnas.1523597113
11. Du XY, Xie XX, Liu RT (2020) The role of alpha-synuclein oligomers in Parkinson's disease. Int J Mol Sci. https://doi.org/10.3390/ijms21228645
12. Okita K, Matsumura Y, Sato Y, Okada A, Morizane A, Okamoto S, Hong H, Nakagawa M, Tanabe K, Tezuka K, Shibata T, Kunisada T, Takahashi M, Takahashi J, Saji H, Yamanaka S (2011) A more efficient method to generate integration-free human iPS cells. Nat Methods 8:409–412. https://doi.org/10.1038/nmeth.1591
13. Li W, Sun W, Zhang Y, Wei W, Ambasudhan R, Xia P, Talantova M, Lin T, Kim J, Wang X, Kim WR, Lipton SA, Zhang K, Ding S (2011) Rapid induction and long-term self-renewal of primitive neural precursors from human embryonic stem cells by small molecule inhibitors. Proc Natl Acad Sci U S A 108:8299–8304. https://doi.org/10.1073/pnas.1014041108
14. Woodard CM, Campos BA, Kuo SH, Nirenberg MJ, Nestor MW, Zimmer M, Mosharov EV, Sulzer D, Zhou H, Paull D, Clark L, Schadt EE, Sardi SP, Rubin L, Eggan K, Brock M, Lipnick S, Rao M, Chang S, Li A, Noggle SA (2014) iPSC-derived dopamine neurons reveal differences between monozygotic twins discordant for Parkinson's disease. Cell Rep 9:1173–1182. https://doi.org/10.1016/j.celrep.2014.10.023
15. Kriks S, Shim JW, Piao J, Ganat YM, Wakeman DR, Xie Z, Carrillo-Reid L, Auyeung G, Antonacci C, Buch A, Yang L, Beal MF, Surmeier DJ, Kordower JH, Tabar V, Studer L (2011) Dopamine neurons derived from human ES cells efficiently engraft in animal models of Parkinson's disease. Nature 480:547–551. https://doi.org/10.1038/nature10648
16. Lees AJ, Hardy J, Revesz T (2009) Parkinson's disease. Lancet 373:2055–2066. https://doi.org/10.1016/S0140-6736(09)60492-X
17. Telenti A, Pierce LC, Biggs WH, di Iulio J, Wong EH, Fabani MM, Kirkness EF, Moustafa A, Shah N, Xie C, Brewerton SC, Bulsara N, Garner C, Metzker G, Sandoval E, Perkins BA, Och FJ, Turpaz Y, Venter JC (2016) Deep sequencing of 10,000 human genomes. Proc Natl Acad Sci U S A 113:11901–11906. https://doi.org/10.1073/pnas.1613365113

18. Lek M, Karczewski KJ, Minikel EV, Samocha KE, Banks E, Fennell T, O'Donnell-Luria AH, Ware JS, Hill AJ, Cummings BB, Tukiainen T, Birnbaum DP, Kosmicki JA, Duncan LE, Estrada K, Zhao F, Zou J, Pierce-Hoffman E, Berghout J, Cooper DN, Deflaux N, DePristo M, Do R, Flannick J, Fromer M, Gauthier L, Goldstein J, Gupta N, Howrigan D, Kiezun A, Kurki MI, Moonshine AL, Natarajan P, Orozco L, Peloso GM, Poplin R, Rivas MA, Ruano-Rubio V, Rose SA, Ruderfer DM, Shakir K, Stenson PD, Stevens C, Thomas BP, Tiao G, Tusie-Luna MT, Weisburd B, Won HH, Yu D, Altshuler DM, Ardissino D, Boehnke M, Danesh J, Donnelly S, Elosua R, Florez JC, Gabriel SB, Getz G, Glatt SJ, Hultman CM, Kathiresan S, Laakso M, McCarroll S, McCarthy MI, McGovern D, McPherson R, Neale BM, Palotie A, Purcell SM, Saleheen D, Scharf JM, Sklar P, Sullivan PF, Tuomilehto J, Tsuang MT, Watkins HC, Wilson JG, Daly MJ, MacArthur DG, Exome Aggregation C (2016) Analysis of protein-coding genetic variation in 60,706 humans. Nature 536:285–291. https://doi.org/10.1038/nature19057
19. Lan T, Lin H, Zhu W, Laurent T, Yang M, Liu X, Wang J, Wang J, Yang H, Xu X, Guo X (2017) Deep whole-genome sequencing of 90 Han Chinese genomes. Gigascience 6:1–7. https://doi.org/10.1093/gigascience/gix067
20. Berman HM, Westbrook J, Feng Z, Gilliland G, Bhat TN, Weissig H, Shindyalov IN, Bourne PE (2000) The protein data bank. Nucleic Acids Res 28:235–242. https://doi.org/10.1093/nar/28.1.235
21. Yachdav G, Kloppmann E, Kajan L, Hecht M, Goldberg T, Hamp T, Honigschmid P, Schafferhans A, Roos M, Bernhofer M, Richter L, Ashkenazy H, Punta M, Schlessinger A, Bromberg Y, Schneider R, Vriend G, Sander C, Ben-Tal N, Rost B (2014) PredictProtein—an open resource for online prediction of protein structural and functional features. Nucleic Acids Res 42:W337–W343. https://doi.org/10.1093/nar/gku366
22. Zhang S, Liu YQ, Jia C, Lim YJ, Feng G, Xu E, Long H, Kimura Y, Tao Y, Zhao C, Wang C, Liu Z, Hu JJ, Ma MR, Liu Z, Jiang L, Li D, Wang R, Dawson VL, Dawson TM, Li YM, Mao X, Liu C (2021) Mechanistic basis for receptor-mediated pathological alpha-synuclein fibril cell-to-cell transmission in Parkinson's disease. Proc Natl Acad Sci U S A. https://doi.org/10.1073/pnas.2011196118
23. Vinueza-Gavilanes R, Inigo-Marco I, Larrea L, Lasa M, Carte B, Santamaria E, Fernandez-Irigoyen J, Bugallo R, Aragon T, Aldabe R, Arrasate M (2020) N-terminal acetylation mutants affect alpha-synuclein stability, protein levels and neuronal toxicity. Neurobiol Dis 137:104781. https://doi.org/10.1016/j.nbd.2020.104781
24. Savyon M, Engelender S (2020) SUMOylation in alpha-synuclein homeostasis and pathology. Front Aging Neurosci 12:167. https://doi.org/10.3389/fnagi.2020.00167
25. Ryan P, Xu M, Davey AK, Danon JJ, Mellick GD, Kassiou M, Rudrawar S (2019) O-GlcNAc modification protects against protein misfolding and aggregation in neurodegenerative disease. ACS Chem Neurosci 10:2209–2221. https://doi.org/10.1021/acschemneuro.9b00143
26. Bluhm A, Schrempel S, von Horsten S, Schulze A, Rossner S (2021) Proteolytic alpha-synuclein cleavage in health and disease. Int J Mol Sci. https://doi.org/10.3390/ijms22115450
27. Nonaka T, Iwatsubo T, Hasegawa M (2005) Ubiquitination of alpha-synuclein. Biochemistry 44:361–368. https://doi.org/10.1021/bi0485528
28. Burmann BM, Gerez JA, Matecko-Burmann I, Campioni S, Kumari P, Ghosh D, Mazur A, Aspholm EE, Sulskis D, Wawrzyniuk M, Bock T, Schmidt A, Rudiger SGD, Riek R, Hiller S (2020) Regulation of alpha-synuclein by chaperones in mammalian cells. Nature 577:127–132. https://doi.org/10.1038/s41586-019-1808-9
29. Sulzer D, Edwards RH (2019) The physiological role of alpha-synuclein and its relationship to Parkinson's disease. J Neurochem 150:475–486. https://doi.org/10.1111/jnc.14810
30. Vasili E, Dominguez-Meijide A, Outeiro TF (2019) Spreading of alpha-synuclein and Tau: a systematic comparison of the mechanisms involved. Front Mol Neurosci 12:107. https://doi.org/10.3389/fnmol.2019.00107
31. Ozansoy M, Basak AN (2013) The central theme of Parkinson's disease: alpha-synuclein. Mol Neurobiol 47:460–465. https://doi.org/10.1007/s12035-012-8369-3
32. Kiely AP, Asi YT, Kara E, Limousin P, Ling H, Lewis P, Proukakis C, Quinn N, Lees AJ, Hardy J, Revesz T, Houlden H, Holton JL (2013) alpha-Synucleinopathy associated with G51D SNCA mutation: a link between Parkinson's disease and multiple system atrophy? Acta Neuropathol 125:753–769. https://doi.org/10.1007/s00401-013-1096-7
33. Konno T, Ross OA, Puschmann A, Dickson DW, Wszolek ZK (2016) Autosomal dominant Parkinson's disease caused by SNCA duplications. Parkinsonism Relat Disord 22(Suppl 1):S1-6. https://doi.org/10.1016/j.parkreldis.2015.09.007
34. Tofaris GK, Kim HT, Hourez R, Jung JW, Kim KP, Goldberg AL (2011) Ubiquitin ligase Nedd4 promotes alpha-synuclein degradation by the endosomal-lysosomal pathway. Proc Natl Acad Sci U S A 108:17004–17009. https://doi.org/10.1073/pnas.1109356108
35. Park GH, Park JH, Chung KC (2021) Precise control of mitophagy through ubiquitin proteasome system and deubiquitin proteases and their dysfunction in Parkinson's disease. BMB Rep 54:592–600. https://doi.org/10.5483/BMBRep.2021.54.12.107
36. Rott R, Szargel R, Haskin J, Bandopadhyay R, Lees AJ, Shani V, Engelender S (2011) alpha-synuclein fate is determined by USP9X-regulated monoubiquitination. Proc Natl Acad Sci U S A 108:18666–18671. https://doi.org/10.1073/pnas.1105725108
37. Kumari R, Kumar R, Kumar S, Singh AK, Hanpude P, Jangir D, Maiti TK (2020) Amyloid aggregates of the deubiquitinase OTUB1 are neurotoxic, suggesting that they contribute to the development of Parkinson's disease. J Biol Chem 295:3466–3484. https://doi.org/10.1074/jbc.RA119.009546